Angiboust, S., and Raimondo, T., 2022, Permeability of subducted oceanic crust revealed by eclogite-facies vugs: Geology, v. 50, https://doi.org/10.1130/G50066.1

Supplementary material for: Angiboust S. and Raimondo T.

Permeability of subducted oceanic crust revealed by eclogite-facies vugs

CONTENT OF THIS FILE

Text S1, S2 and S3

Figures S1 to S5

Table S1

Text S1: Analytical methods

Electron probe microanalysis (EPMA):
Quantitative mineral analyses for garnet and clinopyroxene were performed using a Cameca SX-5 microprobe with five WDS detectors at Sorbonne University, Paris (CAMPARIS facility). Typical analytical conditions of 15kV, 20 nA, and a 1 µm beam were used. X-ray maps were performed at 15kV using a 235 nA intensity, 3µm step size and 60 ms dwell time. Fe_2O_3 (Fe), $MnTiO_3$ (Mn, Ti), diopside (Mg, Si), CaF_2 (F), orthoclase (Al, K), anorthite (Ca) and albite (Na) were used as standards. Clinopyroxene composition is calculated according to the classification of Morimoto (1988).

Laser ablation-inductively coupled plasma-mass spectrometry (LA-ICP-MS) mapping:
LA-ICP-MS trace element maps were acquired using a Resonetics M-50-LR 193 nm excimer laser coupled to an Agilent 7700x Quadrupole ICP-MS housed at Adelaide Microscopy, University of Adelaide. Instrument conditions and mapping protocols similar to that employed in this study are outlined in Raimondo et al. (2017). Pre-ablation of each raster scan was completed to minimize the effect of redeposition (25 µm, 75% overlap), followed by 20 s washout and 10 s of background measurement. A beam diameter of 25 µm, line spacing of 25 µm and repetition rate of 10 Hz were used, resulting in an energy density of 3.5 J/cm^2 at the target. Standards were analyzed in duplicate every 2 h during the mapping session, including reference glasses NIST 612 (Pearce et al., 1997; Jochum et al., 2011a) and GSD-1D (Jochum et al., 2011b). A beam diameter of 43 µm was used for all standard analyses, and included 5 pre-ablation shots (43 µm, 75% overlap) followed by 20 s washout, 30 s background measurement and 40 s ablation time. Data acquisition was performed in time-resolved analysis mode as a single continuous experiment. Each analysis comprised a suite of 31 elements, and dwell times were as follows: 0.002 s (Mg, Al, Si, P, Ca, Mn, Fe), 0.005 s (Ti, V, Cr, Hf, Pb, Th, U), 0.008 s (Y, Zr, La, Ce, Pr, Ho, Er, Tm, Yb, Lu), 0.01 s (Li, Nd, Tb, Dy) and 0.015 s (Sm, Eu, Gd). Post-acquisition processing was performed using the software Iolite (Woodhead et al., 2007; Hellstrom et al., 2008; Paton et al., 2011), with data reduction and image processing procedures following those outlined by Raimondo et al. (2017).

Text S2: Pseudosection modelling approach

To constrain phase relationships during burial as a function of the available H_2O content for sample VI0917, a pseudosection was calculated using a Gibbs free energy minimization approach using the software *Perplex* (Connolly, 2005; version 6.7.4) and the internally-consistent Holland & Powell (2011) dataset in the Na_2O-CaO-K_2O-FeO-MgO-Al_2O_3-SiO_2-H_2O-O_2 (NCKFMASHO) chemical system. Activity-composition models were used for the following phases: garnet (White et al., 2007), clinopyroxene (Green et al., 2007), clinoamphibole (Diener & Powell, 2012), white mica (Coggon and Holland, 2002), chlorite (Holland et al., 1998), epidote (Holland and Powell, 1998) and feldspar (Fuhrman and Lindsley, 1988). Given that rutile is predicted over the entire P/T-H_2O domain studied, TiO_2 has been neglected. The bulk composition for sample VI0917 is derived from Angiboust et al. (2012), calculated by combining single EPMA point analyses and estimated mineral proportions. The normalized composition is as follows: SiO_2 (53.2), Al_2O_3 (14.7), FeO (7.9), Fe_2O_3 (0.4), MgO (6.1), CaO (11.5), Na_2O (5.9), and K_2O (0.3). The amount of ferric iron in the system is arbitrarily set to a low value of 5% ($XFe_2O_3=Fe_2O_3/(Fe_2O_3+FeO)$, mol.%), as indicated by the low aegyrine content of peak burial clinopyroxene (see Angiboust et al., 2012 for further petrological details and mineral chemistry). This value, although challenging to precisely constrain in deep-seated metamorphic systems due to the superposition of inherited and introduced sources of Fe^{3+} from prograde to exhumation metamorphic stages, also yields the best fit between modelled and observed mineral compositions and proportions. The fluid phase is assumed to be pure H_2O because carbonates are absent from the studied Monviso metagabbro.

Given the fine-grained nature of the mylonitic host and the complex garnet zoning patterns, potential fractionation effects that existed during garnet growth were neglected for the sake of simplicity. Manganese, despite its importance in stabilizing garnet cores towards lower temperatures, has also been neglected for simplicity in the first instance because of its low concentration in the host bulk composition (~0.27 wt.% MnO). In a second model, however, we evaluated the effect on phase relationships of incorporating Mn as a system component (see Fig. S5). This change (i) decreases the Grt-in line by c. 20 °C; and (ii) broadens the *T* window where eclogitization-related fluids are released (from 15 to 30 °C). Because Mn strongly fractionates into garnet cores (Mahar et al., 1997), estimating the actual effective Mn content available for reaction approaching peak burial conditions is impossible. In addition, garnet nucleation is known to be potentially delayed during burial because of overstepping processes (e.g. Spear, 2017 and references therein). Considering these kinetic effects, it is thus acknowledged that the width of the dehydration *T* window lies between 15 °C and 30 °C. This uncertainty is commensurate with the error range classically envisioned for thermodynamic models (between ±10 and ±40 °C; Angiboust et al., 2012; Palin et al., 2016).

Text S3: Permeability calculation approach

Based on Perplex software fluid production results (~3 wt.% H_2O produced by the eclogitization reactions; Fig. 3c), we derive a fluid production term F on the order of 10^{-6} $m^3/(m^2.yr)$ for a characteristic meter-sized length scale of the dehydrating eclogitic volume and integrated over

the inferred 1 Ma duration of the fluid expulsion event (see Fig. 4 and the text for details; see also Hyndman & Peacock, 2003). The permeability κ (in m²) is obtained by the following equation, which directly derives from Darcy's law (see Peacock et al., 2011 for calculation details):

$$\kappa \text{ (in m}^2\text{)} = F\ (\eta / \rho g)$$

where η is the fluid dynamic viscosity at 500 °C (fixed here at 0.0001 Pa.s), ρ the water density of 1230 kg/m^3 (data derived from Perplex calculations at peak burial conditions) and g the gravity acceleration constant. These calculations yield permeability values κ on the order of 10^{-22} m², which represent an upper bound for eclogite permeability in order to maintain the fluid trapped in a vug over the spatial and temporal scales considered here.

Figure S1: Geological map and cross section of the study area (modified after Rubatto & Angiboust, 2015).

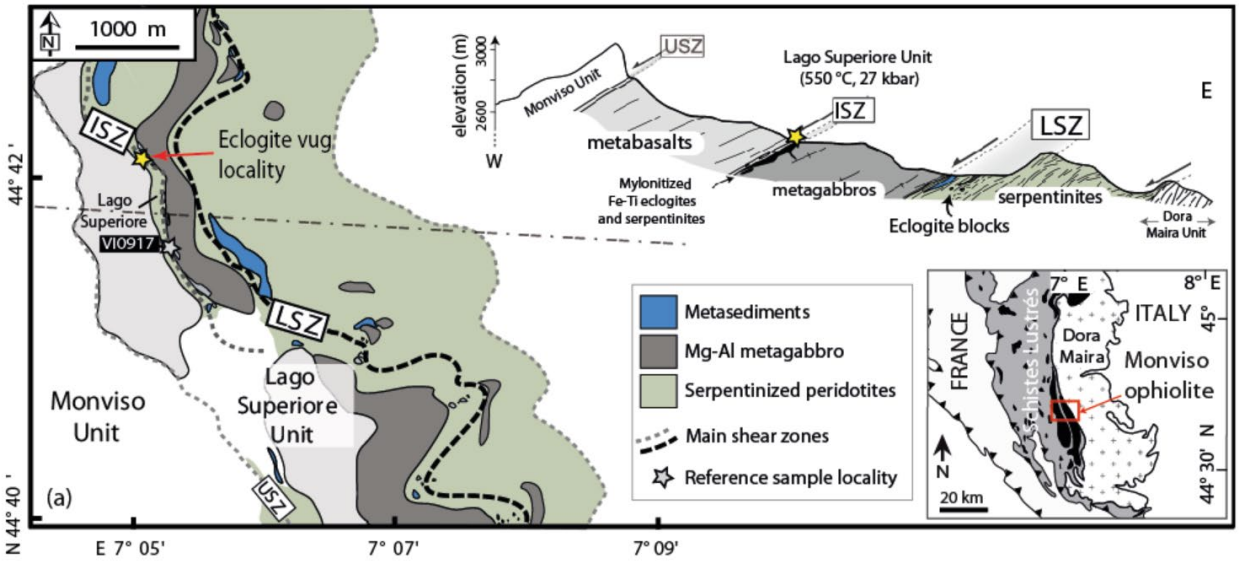

Figure S2: Ternary diagrams for clinopyroxene and garnet

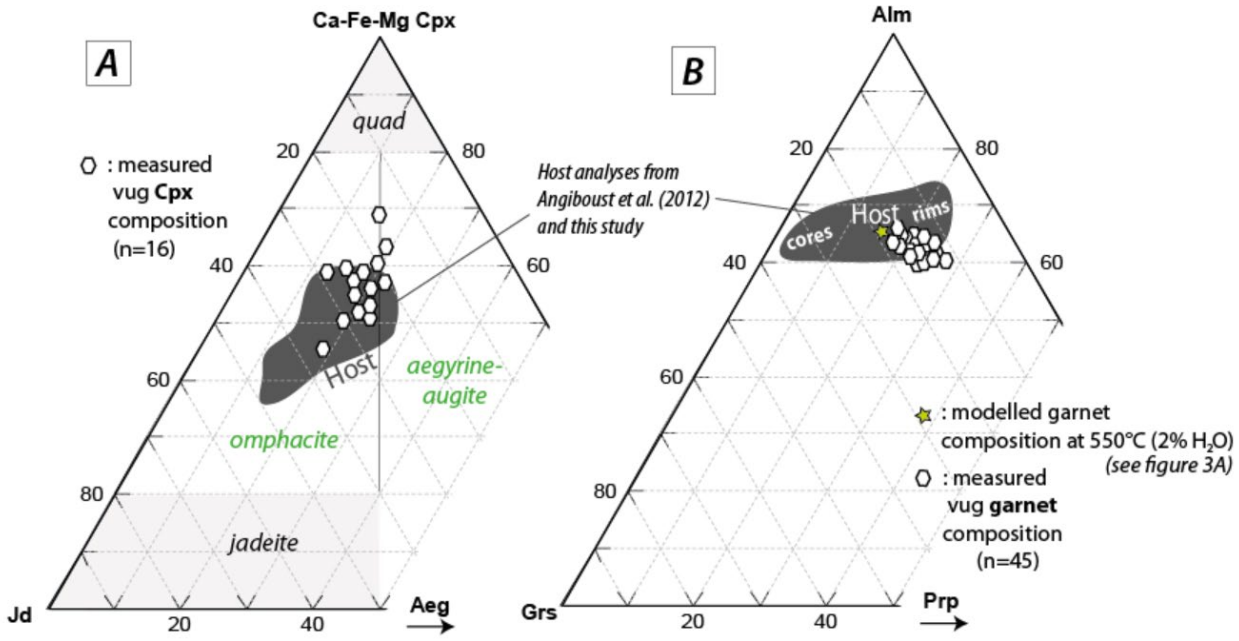

Figure S3: Additional X-ray maps of the vug-host contact

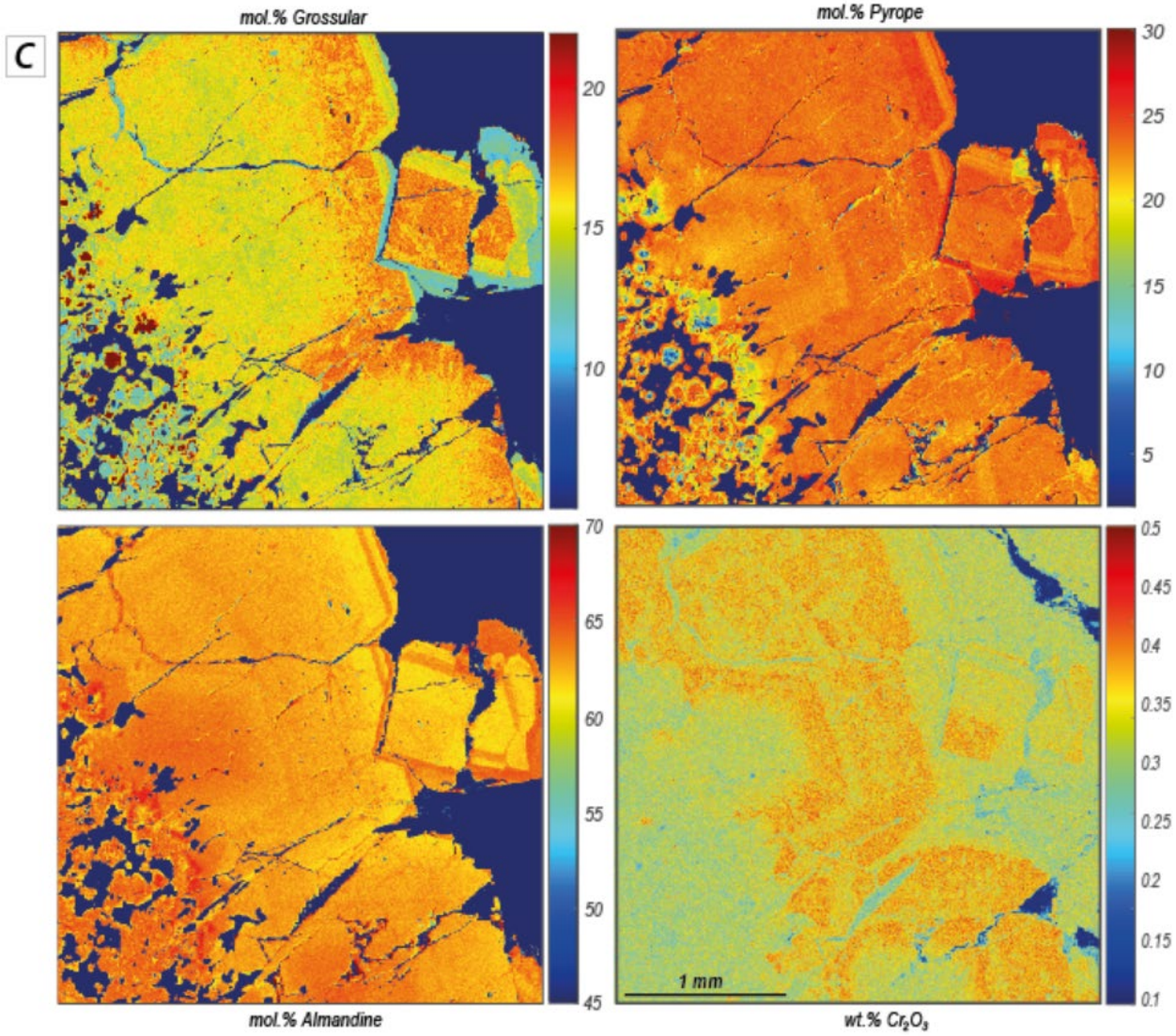

Figure S4: Complete LA-ICP-MS maps of the vug-host contact *(sample VI1805b)*

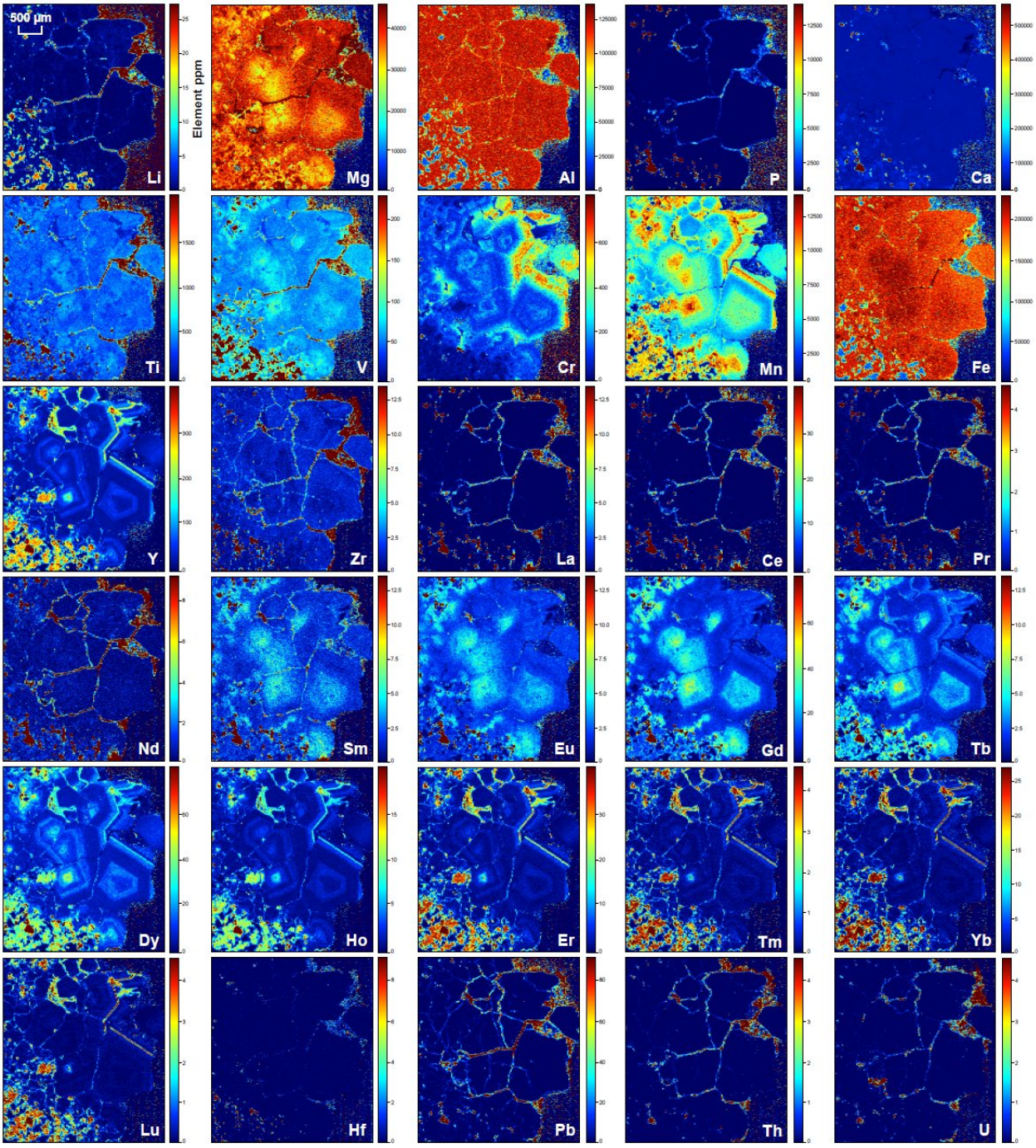

Figure S5: Effect of Mn on thermodynamically modelled phase proportions

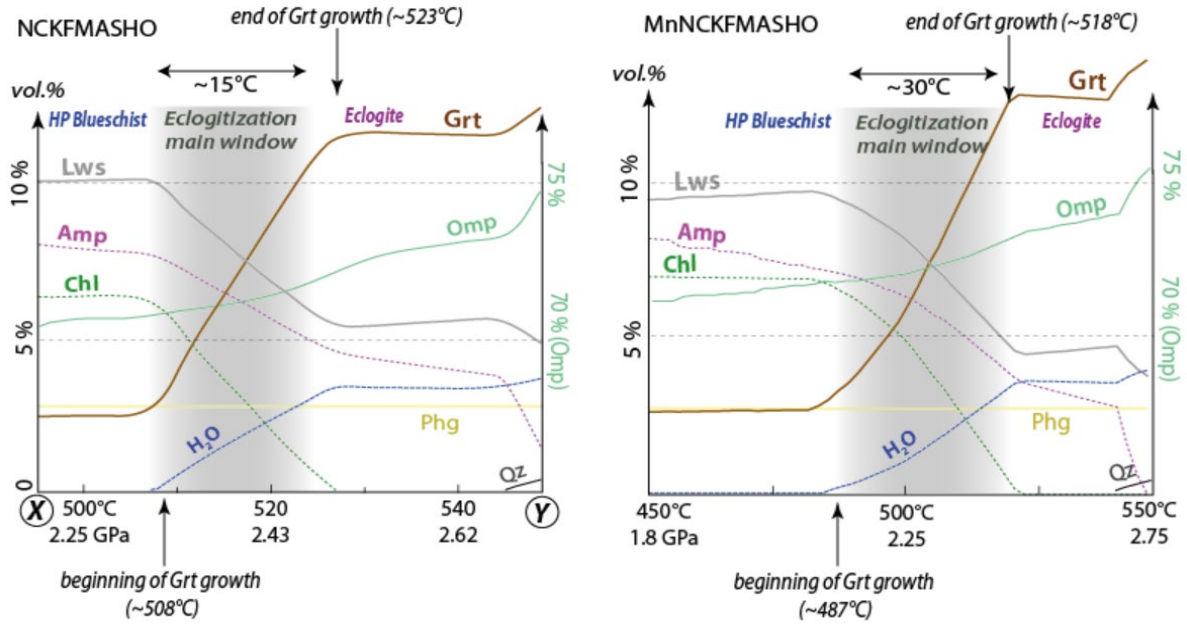

Table S1: Representative electron probe mineral analyses (wt.%)

	Cpx vug ***#33***	***Cpx*** vug ***#36***	***Cpx*** host ***#41***		***Grt*** vug ***#28***	***Grt*** vug ***#27***	***Grt*** host ***#38***	***Grt*** host ***#39***	***Grt*** host ***#37***
SiO_2	54.99	54.92	54.62		38.61	38.82	37.76	38.18	38.28
TiO_2	0.07	0.03	0.10		0.05	0.03	0.03	0.09	0.05
Al_2O_3	9.53	5.27	5.99		21.50	21.42	21.57	21.03	21.39
FeO	6.49	9.35	9.30		28.77	27.83	29.20	29.40	28.16
MnO	0.05	bdl	bdl		1.10	1.42	1.04	1.29	1.24
MgO	8.30	9.78	9.07		6.85	6.25	6.06	6.63	6.50
CaO	12.07	15.05	14.11		4.33	5.43	5.55	4.37	5.25
Na_2O	7.69	6.12	6.64		bdl	0.02	0.02	0.03	0.02
K_2O	0.06	bdl	0.00		bdl	bdl	0.01	bdl	bdl
Cr_2O_3	0.09	bdl	0.03		0.02	0.10	bdl	0.03	0.02
Total	99.33	100.53	99.87		101.25	101.31	101.24	101.06	100.91

Quad	*46*	*57*	*53*	*Alm*	*60*	*59*	*61*	*60*	*59*
Jd	*36*	*20*	*23*	*Prp*	*26*	*24*	*22*	*25*	*24*
Aeg	*18*	*23*	*24*	*Grs*	*12*	*14*	*15*	*12*	*14*
				Sps	*2*	*3*	*2*	*3*	*3*

References:

Angiboust, S., Langdon, R., Agard, P., Waters, D., & Chopin, C. (2012). Eclogitization of the Monviso ophiolite (W. Alps) and implications on subduction dynamics. *Journal of Metamorphic Geology*, 30(1), 37-61.

Coggon, R., & Holland, T. J. B. (2002). Mixing properties of phengitic micas and revised garnet-phengite thermobarometers. *Journal of Metamorphic Geology*, 20(7), 683-696.

Connolly, J. A. (2005). Computation of phase equilibria by linear programming: a tool for geodynamic modeling and its application to subduction zone decarbonation. *Earth and Planetary Science Letters*, 236(1-2), 524-541.

Diener, J. F. A., & Powell, R. (2012). Revised activity–composition models for clinopyroxene and amphibole. *Journal of Metamorphic Geology*, 30(2), 131-142.

Fuhrman, M. L., & Lindsley, D. H. (1988). Ternary-feldspar modeling and thermometry. *American mineralogist*, 73(3-4), 201-215.

Green, E., Holland, T., & Powell, R. (2007). An order-disorder model for omphacitic pyroxenes in the system jadeite-diopside-hedenbergite-acmite, with applications to eclogitic rocks. *American Mineralogist*, 92(7), 1181-1189.

Groppo, C., & Castelli, D. (2010). Prograde P–T evolution of a lawsonite eclogite from the Monviso meta-ophiolite (Western Alps): dehydration and redox reactions during subduction of oceanic FeTi-oxide gabbro. *Journal of Petrology*, 51(12), 2489-2514.

Jochum, K. P., Wilson, S. A., Abouchami, W., Amini, M., Chmeleff, J., Eisenhauer, A., ... & Woodhead, J. D. (2011). GSD-1G and MPI-DING reference glasses for in situ and bulk isotopic determination. *Geostandards and Geoanalytical Research*, 35(2), 193-226.

Hellstrom, J., Paton, C., Woodhead, J., & Hergt, J. (2008). Iolite: software for spatially resolved LA-(quad and MC) ICPMS analysis. *Mineralogical Association of Canada short course series*, 40, 343-348.

Holland, T.J.B., Powell, R. (2011). An internally consistent thermodynamic data set for phases of petrological interest. *Journal of Metamorphic Geology,* 16, 309–343.

Holland, T. J. B., & Powell, R. T. J. B. (1998). An internally consistent thermodynamic data set for phases of petrological interest. *Journal of metamorphic Geology*, 16(3), 309-343.

Holland, T., Baker, J., & Powell, R. (1998). Mixing properties and activity-composition relationships of chlorites in the system MgO-FeO-Al2O3-SiO2-H2O. *European Journal of Mineralogy*, 395-406.

Hyndman, R. D., & Peacock, S. M. (2003). Serpentinization of the forearc mantle. *Earth and Planetary Science Letters*, 212(3-4), 417-432.

Mahar, E. M., Baker, J. M., Powell, R., Holland, T. J. B., & Howell, N. (1997). The effect of Mn on mineral stability in metapelites. *Journal of Metamorphic Geology*, 15(2), 223-238.

Morimoto, N. (1988). Nomenclature of pyroxenes. *Mineralogy and Petrology*, 39(1), 55-76.

Palin, R. M., Weller, O. M., Waters, D. J., & Dyck, B. (2016). Quantifying geological uncertainty in metamorphic phase equilibria modelling; a Monte Carlo assessment and implications for tectonic interpretations. *Geoscience Frontiers*, 7(4), 591-607.

Paton, C., Hellstrom, J., Paul, B., Woodhead, J., & Hergt, J. (2011). Iolite: Freeware for the visualisation and processing of mass spectrometric data. *Journal of Analytical Atomic Spectrometry*, 26(12), 2508-2518.

Peacock, S. M., Christensen, N. I., Bostock, M. G., & Audet, P. (2011). High pore pressures and porosity at 35 km depth in the Cascadia subduction zone. *Geology*, 39(5), 471-474.

Pearce, N. J., Perkins, W. T., Westgate, J. A., Gorton, M. P., Jackson, S. E., Neal, C. R., & Chenery, S. P. (1997). A compilation of new and published major and trace element data for NIST SRM 610 and NIST SRM 612 glass reference materials. *Geostandards newsletter*, 21(1), 115-144.

Raimondo, T., Payne, J., Wade, B., Lanari, P., Clark, C., & Hand, M. (2017). Trace element mapping by LA-ICP-MS: assessing geochemical mobility in garnet. *Contributions to mineralogy and petrology*, 172(4), 1-22.

Rubatto, D., & Angiboust, S. (2015). Oxygen isotope record of oceanic and high-pressure metasomatism: a P–T–time–fluid path for the Monviso eclogites (Italy). *Contributions to mineralogy and petrology*, 170(5), 1-16.

Spear, F. S. (2017). Garnet growth after overstepping. *Chemical Geology*, 466, 491-499.

White, R. W., Powell, R., & Holland, T. J. B. (2007). Progress relating to calculation of partial melting equilibria for metapelites. *Journal of metamorphic Geology*, 25(5), 511-527.

Whitney, D. L., & Evans, B. W. (2010). Abbreviations for names of rock-forming minerals. *American mineralogist*, 95(1), 185-187.

Woodhead, J. D., Hellstrom, J., Hergt, J. M., Greig, A., & Maas, R. (2007). Isotopic and elemental imaging of geological materials by laser ablation inductively coupled plasma-mass spectrometry. *Geostandards and Geoanalytical Research*, 31(4), 331-343.